Dielectronic excitation of Ne *K*-shell electrons in 2–170-keV N^{7+}+Ne collisions

C. Bedouet, F. Frémont, J. Y. Chesnel, X. Husson, and H. Merabet*
Centre Interdisciplinaire de Recherche Ions-Lasers, Unité Mixte CEA-CNRS-ISMRA Université, 6 Boulevard du Maréchal Juin, F-14050 Caen Cedex, France

N. Vaeck and N. Zitane
Laboratoire de Chimie Physique Moléculaire, Code Postal 160/09, Université Libre de Bruxelles, 50 avenue F. Rossevelt, B-1050 Bruxelles, Belgium

B. Sulik
Institute of Nuclear Research of the Hungarian Academy of Sciences, P.O. Box 51, H-4001 Debrecen, Hungary

M. Grether, A. Spieler, and N. Stolterfoht
Hahn-Meitner Institut, Bereich Festkörperphysik, Glienicker Strasse 100, D-14109 Berlin, Germany
(Received 24 November 1998)

We report on the projectile energy dependence of the cross sections for producing *K* Auger electrons in 2–170-keV N^{7+}+Ne collisions. The present studies, which extend previous work performed at the impact energy of 35 keV, give evidence for a dielectronic excitation process produced by electron-electron interaction. At impact energies in the range 5–170 keV, the cross sections are found to be larger than $10^{-17}\,cm^2$. Molecular-orbital energy diagrams were determined to analyze details of the collision. Analytic models were used to evaluate cross sections associated with dielectronic excitation. The results show good agreement with experiment. The dielectronic excitation process is dominant when three electrons from the target are transferred into an excited state of the projectile. [S1050-2947(99)05306-8]

PACS number(s): 32.80.Hd, 34.50.−s

I. INTRODUCTION

In the last two decades, considerable work has been devoted to multiple-electron capture in collisions of slow highly charged ions on few-electron target atoms [1–5]. Particularly, the study of double-electron capture has received a great deal of attention. Mechanisms responsible for double capture have been extensively studied experimentally and theoretically [2,4–11]. Specific effort has been devoted to electron correlation effects [6,12,13]. These effects are produced by mutual interaction of two electrons which causes deviations from the prediction of the independent particle model. A characteristic example of dielectronic processes, associated with dynamic electron correlation, is autoexcitation, where one electron is transferred from the target to a deeper level of the projectile, while another electron is excited to a higher Rydberg state. Examples for autoexcitation processes occurring during the collision are the processes of correlated double capture (CDC) [2,6,12] and correlated transfer excitation (CTE) [13].

Double capture processes have been extensively analyzed in the case of a helium target. It has been commonly accepted that, in most collision systems [14–16], configurations of (near-) equivalent electrons $nln'l'$ $(n'\approx n)$ can be produced by independent monoelectronic transitions caused by electron-nucleus interaction. For example, in the case of the system Ne^{10+}+He at a projectile velocity of 0.5 a.u., the configurations $3ln'l'$ $(n'=4-5)$ are populated by monoelectronic processes [16]. However, in specific cases, it was shown that configurations of near-equivalent electrons can also be populated by dielectronic processes due to electron correlation [4]. The situation is different for configurations of nonequivalent electrons $nln'l'$ $(n'\gg n)$. The production of such configurations was uniquely attributed to dielectronic mechanisms [2]. As a recent example, for the Ne^{10+}+He collision system at a projectile velocity of 0.5 a.u., the configurations $3ln'l'$ $(n'\geqslant 6)$ were shown to be populated by dielectronic processes [16].

Here we focus our attention on the inverse autoexcitation process, also referred to as *dielectronic excitation* [17]. Due to electron-electron interaction, an electron from a higher-lying level is deexcited, transferring its excess energy to another electron which, in turn, is removed from a deeper-lying level. It is noted that this process is dominant at low collision energies, at which ionization and excitation fail to produce inner-shell vacancies. The first indication for dielectronic excitation has been provided by Afrosimov *et al.* [18] studying the singly charged system N^++Ar. Similar measurements of vacancy creation in the *L* shell of the heavier collision partner in the collision Ar^++Si have also been performed [19]. In this latter example, a promotion of two *L*-shell electrons of Si occurs, so that resonance conditions are created for the inverse autoexcitation process. Thus, the two vacancies are simultaneously filled by transitions from a higher-lying orbital and an electron from the $2p$ orbital of Ar. This dielectronic excitation process has been confirmed by model calculations [20].

Recently, we provided clear experimental evidence for the

*Present address: Department of Physics/220, University of Nevada, Reno, NV 89557-0058.

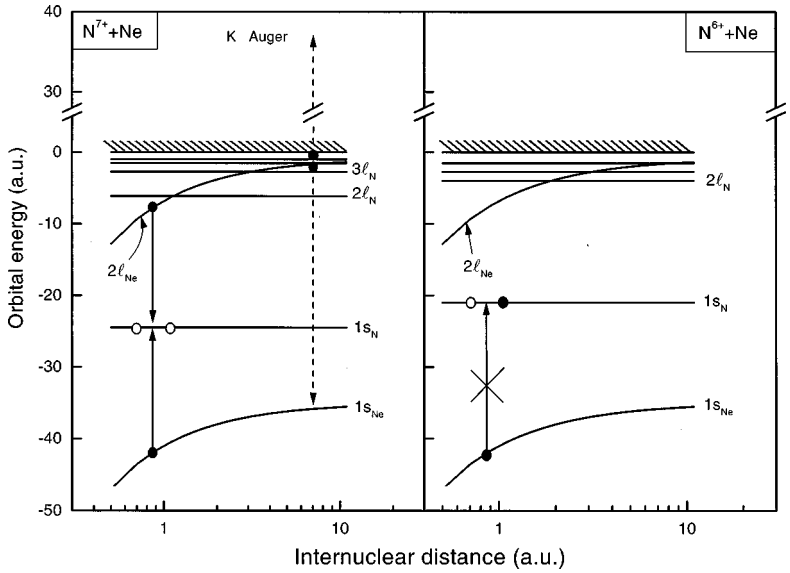

FIG. 1. Diagram of orbital energies for the systems $N^{6+}+Ne$ and $N^{7+}+Ne$. In $N^{7+}+Ne$ collisions (left diagram), resonance conditions lead to a simultaneous transfer of a 1*s*- and a 2*l*-target electron by means of dielectronic excitation. This process produces target configurations decaying by *K* Auger-electron emission (dashed lines). In $N^{6+}+Ne$ (right diagram), Ne *K*-shell excitation is unexpected, since electron transfer from the 1*s* orbital of Ne to the 1*s* orbital of N can be excluded at low collision energies.

dielectronic excitation process when multiply charged ions are used as projectiles [21]. In that study, the collision system 35-keV $N^{7+}+Ne$ was investigated by means of Auger-electron spectroscopy. The mechanism of dielectronic excitation can be understood in terms of the orbital energy-curve diagram shown in Fig. 1, which illustrates resonance conditions for electron transfer in $N^{6+}+Ne$ and $N^{7+}+Ne$ collisions [21]. In the incident channel, two electrons occupy the Ne-1*s* orbital and eight electrons fill the Ne-2*l* orbital. In both collision systems, the Ne-1*s* orbital does not cross the orbitals of the projectile. Thus, the capture of a 1*s*-target electron by means of a *single*-electron transition is very unlikely in both systems.

In the case of the $N^{7+}+Ne$ collision (left side of Fig. 1), it is seen that at internuclear distances of $\sim$1 a.u. resonance conditions are created for the dielectronic excitation process in which a 2*l* and a 1*s* electron from the Ne target are simultaneously transferred into the 1*s* orbital of the N projectile. The presence of two 1*s* vacancies initially in the projectile is essential for the dielectronic excitation process. Thus, it is clear that the dielectronic excitation process is unlikely for the $N^{6+}+Ne$ collision system (right side of Fig. 1) since the 1*s*-projectile orbital is already occupied by one electron.

After the dielectronic excitation process in the $N^{7+}+Ne$ system, the target is in an excited state with a vacancy in the *K* shell. Hence, the target may decay via *K* Auger-electron emission. Therefore, the dielectronic process can be studied by means of target Auger-electron spectroscopy. It is important to note that the peaks corresponding to the dielectronic excitation process are well separated from Auger peaks due to other mechanisms which may contribute to electron capture in $N^{7+}+Ne$ collision [21].

In the case of systems involving multiply charged ions such as C^{6+} or Ne^{10+} and a He target [22,23], the relative contribution of the dielectronic processes versus that of the monoelectronic processes was shown to be significantly enhanced when the projectile energy decreases. In Fig. 2 capture cross sections calculated by means of the Landau-Zener model [24] and associated with two different capture channels for the system $Ne^{10+}+He$ are reported as a function of projectile velocity. In the case of monoelectronic transitions (dashed curve in Fig. 2), the coupling matrix element V_{if} is of the order of 0.3 a.u. Thus, according to the Landau-Zener model [24], the corresponding cross section exhibits a maximum at relatively large impact velocities ($\sim$2 a.u. in Fig. 2).

In contrast to the monoelectronic interactions, the

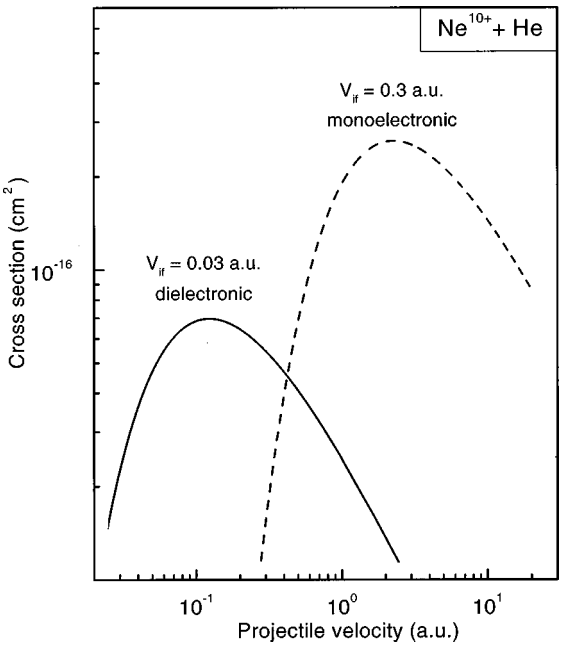

FIG. 2. Cross sections calculated using the Landau-Zener model for single-electron capture (dashed curve) and double-electron capture due to electron-electron interaction (full curve) in $Ne^{10+}+He$ collisions, as a function of impact velocity. Typical matrix elements (labeled V_{if}) for monoelectronic and dielectronic couplings are given.

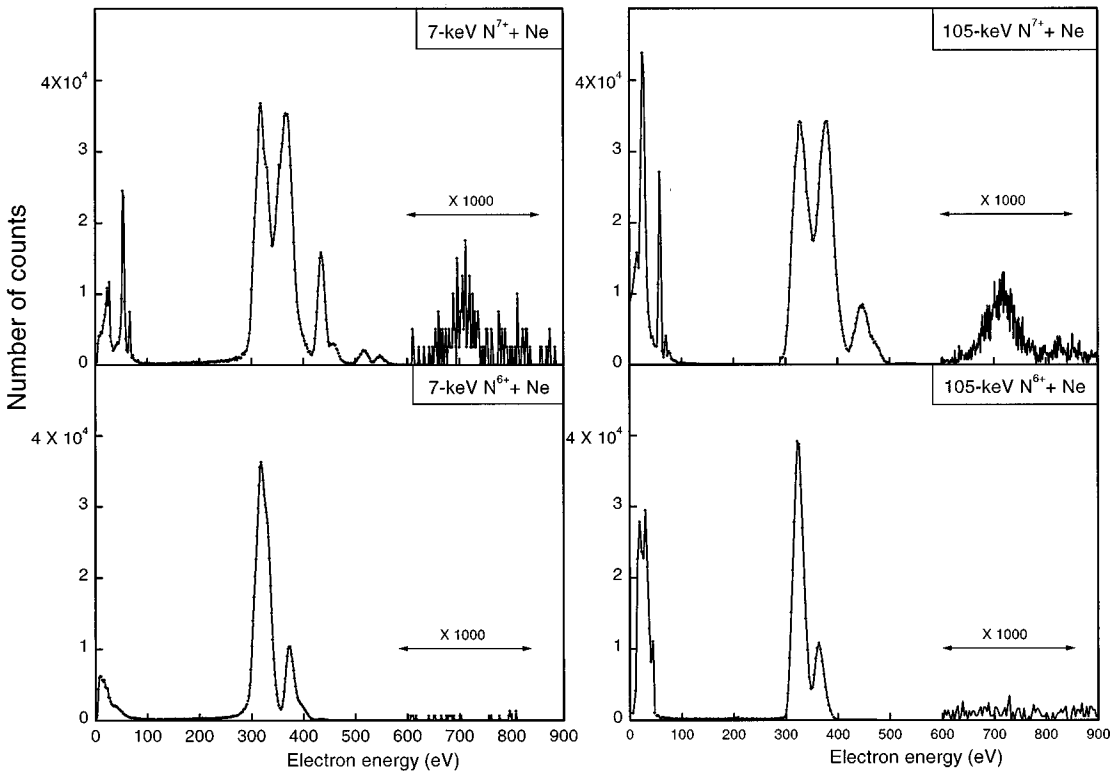

FIG. 3. Spectra of Auger electrons produced in 7- and 105-keV N^{6+}+Ne and N^{7+}+Ne collisions at an observation angle of 150°. The peaks in the range 0–500 eV correspond to the decay of multiexcited states of the projectile [21]. The group of peaks centered at ~710 eV in N^{7+}+Ne collisions is produced by dielectronic excitation, which simultaneously creates a vacancy in the *K* shell of the target and a transfer of a $2l$-target electron. It is seen that the collision N^{6+}+Ne does not create a *K* vacancy in the target.

electron-electron interaction is small (V_{if} is of the order of 0.03 a.u.). The maximum for the cross sections (full line in Fig. 2) is thus shifted to lower impact velocities. Consequently, dielectronic processes are likely to be dominant at very low impact velocities (~0.05 a.u.). Thus, in the present paper, the objective is to perform a comprehensive study of the dielectronic excitation process in the N^{7+}+Ne system at collision velocities from 0.67 down to 0.07 a.u. (i.e., at impact energies from 170 down to 2 keV, respectively). Since the *K* Auger emission following a *K* neon vacancy production is dominant [25], the experiments were performed using the method of Auger-electron spectroscopy.

The paper is structured as follows. Experimental method and Auger spectra are presented in Sec. II. In Sec. III, Auger emission cross sections resulting from *K* neon vacancy are evaluated. Auger yields for each configuration of the ionized target are also determined. Average Auger yields are then deduced to extract total cross sections. In Sec. IV, molecular-orbital diagrams are given. Using these diagrams, Landau-Zener calculations were performed to evaluate cross sections associated with the dielectronic excitation process. From the comparison with experimental results, the dielectronic mechanism is further discussed.

II. EXPERIMENTAL METHOD

The measurements were carried out at the 14-GHz electron cyclotron resonance (ECR) ion sources at the Grand Accélérateur National d'Ions Lourds (GANIL) in Caen and at the Ionenstrahl-Labor of the Hahn-Meitner Institut (HMI) in Berlin. Higher-energy beams were achieved in Caen, while beams of energies below 35 keV were produced in Berlin. Beam energies lower than 10 keV were realized using the advanced beam-deceleration method installed at the ECR source of HMI. Ions of N^{7+} were extracted from the ECR source and collimated to a diameter of ~2 mm, with typical currents of about 30 nA. In the collision chamber, the beam was colliding with an effusive Ne-gas jet target. During the acquisition, the pressure of $\sim 3\times 10^{-5}$ Torr was maintained in the chamber. This pressure was sufficiently low to avoid multiple charge-exchange collisions for the incident ions.

Auger electrons produced in N^{7+}+Ne collisions were measured at detection angles of 120° and 150°, with respect to the incident beam direction, using a single stage spectrometer developed at HMI which consists of an electrostatic parallel-plate analyzer [26]. The resolution of the analyzer was 5% full width at half maximum (FWHM). At the exit of the spectrometer the Auger electrons were detected by a channeltron electron multiplier.

Figure 3 shows typical Auger-electron spectra for the systems N^{6+} and N^{7+}+Ne at 7- and 105-keV projectile energies. Peaks in the energy range 20–500 eV are attributed to electrons emitted by the projectile [21]. As mentioned previously, double-electron capture populates configurations of near-equivalent electrons $3lnl'$ and $4lnl'$ ($n\geqslant 4$), which give rise to *L* Auger electrons in the range 0–100 eV (Fig. 3). The line intensities in the range 200–500 eV are essentially due to capture into triply excited states.

For the particular case of the N^{7+}+Ne system, Auger peaks in the range 600–900 eV are observed at both projec-

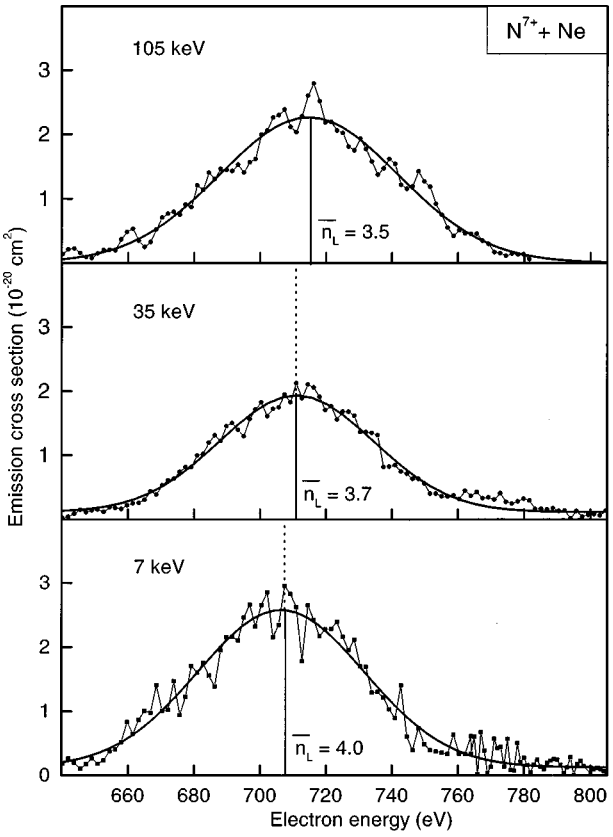

FIG. 4. Spectra of Auger electrons produced in N^{7+}+Ne collisions at projectile energies of 7, 35, and 105 keV. The peaks correspond to the *K* Auger decay of the target. Gaussian curves are used to fit the spectra (full line). From the fit procedure, the centroid energy of the peaks is deduced (vertical lines).

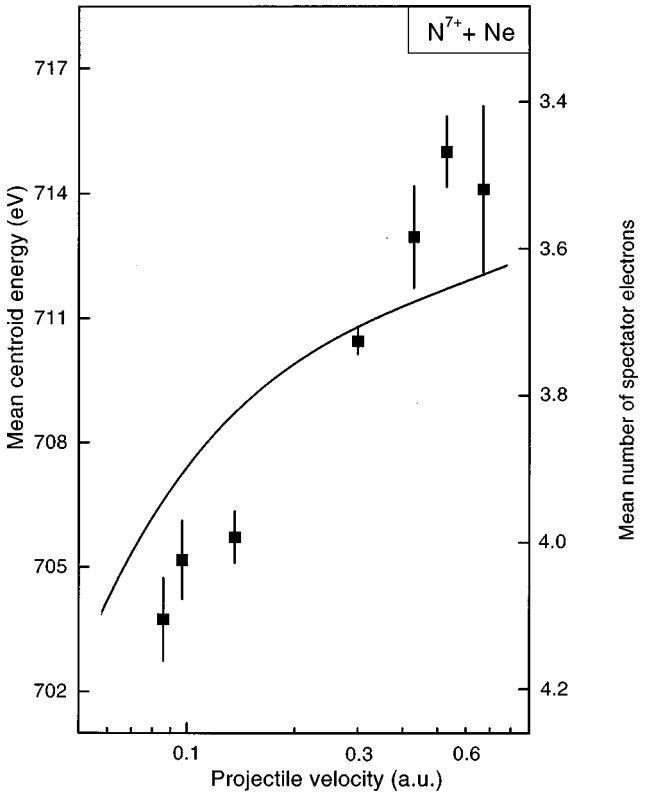

FIG. 5. Mean centroid energy $\overline{E_C}$ (squares) of the Ne Auger peaks as a function of the projectile velocity. The associated mean number $\overline{n_L}$ of spectator electrons is also given (right side of the figure). The full line represents the result of the present model calculations.

tile energies. This is attributed to the occurrence of dielectronic excitation, where two $1s$- and $2l$-target electrons are transferred into the $1s$-projectile orbital due to electron-electron interaction (see Fig. 1 and Ref. [21]). Thus, a vacancy is created in the *K* shell of the target. After the collision, the target deexcites by emission of a *K* Auger electron.

As mentioned in the Introduction, two $1s$ vacancies in the projectile are essential for the occurrence of the dielectronic excitation process. In the N^{6+}+Ne system, a $1s$-projectile orbital is already occupied by one electron, so that the dielectronic process is impossible. It is clearly seen in Fig. 3 that *K* Auger target electrons are not detected when N^{6+} is used as a projectile. As noted previously for other collision systems [27], the Auger electrons from the neon target ($\sim$700 eV) are influenced by the azimuthal broadening effect produced by the random direction of the recoil momentum. This effect is particularly large at low impact velocities, as shown in Fig. 4. At 7 keV the azimuthal line broadening was estimated to be $\sim$18 eV at an observation angle of 150°. Consequently, fine structures of the spectrum are not visible.

III. ANALYSIS OF THE SPECTRA

As seen in Fig. 4, the wide energy range of the Auger spectrum (600–800 eV) indicates that the spectrum exhibits a large number of overlapping lines. These lines originate from the transfer of n_L *L*-shell target electrons ($0 \leqslant n_L \leqslant 5$ for the present system) in addition to the dielectronic excitation process. In the following, these *L*-shell electrons will be referred to as *spectator electrons* while the electrons which interact by means of dielectronic excitation will be called *active electrons*.

Information about the mean number $\overline{n_L}$ can be extracted from the mean centroid energy $\overline{E_C}$ of the *K* Auger-electron peak at the different impact velocities (Fig. 4). To determine the experimental centroid energy $\overline{E_C}$, the spectra were fitted by Gaussian curves (Fig. 4). In the entire range of the studied projectile velocities it is seen that the group of peaks is centered at about 710 eV. From the relationship previously given [27], this centroid energy corresponds to an $\overline{n_L}$ value of about 3.5.

It is also seen that $\overline{E_C}$ is shifted to lower energies (Fig. 4) when the projectile velocity decreases. Typically, the measured shift is of the order of 10 eV when the projectile velocity varies from 0.09 to 0.7 a.u. (Fig. 5). Note that this value is significantly larger compared to the experimental uncertainties of the Auger-electron energy. For example, the experimental error of $\overline{E_C}$ at the velocity of $\sim$0.6 a.u. was found to be smaller than 1 eV. Hence, as $\overline{E_C}$ varies noticeably, the mean number $\overline{n_L}$ is found to increase from about 3 to 4 when the projectile velocity decreases from 0.7 down to 0.09 a.u. (Fig. 5).

To obtain information on the projectile-velocity dependence of the dielectronic process, Auger emission cross sections were determined. Single-differential cross sections

TABLE I. Auger emission cross sections σ^a for producing neon *K* vacancy in 2–167-keV N^{7+}+Ne collisions. The experimental uncertainties are about 20% (see text). The mean number $\overline{n_L}$ of spectator electrons is derived from the relationship given in Ref. [27].

v_p (a.u.)	σ^a (10^{-17} cm^2)	$\overline{n_L}$
0.075	0.7±0.3	4.0
0.086	0.95±0.20	4.0
0.11	1.0±0.2	3.9
0.14	2.1±0.4	3.9
0.30	1.6±0.3	3.7
0.43	2.2±0.4	3.7
0.53	1.9±0.4	3.6
0.67	1.4±0.3	3.6

$d\sigma^a/d\Omega$ for Auger-electron emission were evaluated by integration of the spectra with respect to electron energy. Assuming an isotropic emission of the target Auger electrons, total Auger-electron emission cross section σ^a was derived by multiplying $d\sigma^a/d\Omega$ by 4π. The isotropy was observed for the particular projectile energy of 35 keV.

The results are presented in Table I [28]. The experimental errors for the cross sections are estimated to be about ±20%. These errors account for uncertainties due to statistics and background subtraction. Moreover, difficulties due to beam deflection were encountered to normalize the spectra at the projectile energies lower than 3 keV. Hence, for these energies the uncertainties are about ±30%. Auger emission cross sections are found to slowly increase with decreasing projectile velocity in the range 0.14–0.67 a.u. (7–167 keV). At velocities lower than 0.14 a.u. the cross sections decrease significantly.

The radiative and nonradiative decay rates for the states $|1s2l^{m_L}J\rangle$ were calculated to determine the associated individual Auger yields $a_{n_L}(1s2l^{m_L})$ for a given n_L value. The exponent m_L refers to the number of $2l$ electrons which remain on the target after the removal of the n_L electrons and the transfer of the $2l$ active electron. The calculations were carried out using the suite of Hartree-Fock (HF) programs written by Cowan [29]. The relativistic option has been used in which the monoelectronic mass correction and the Darwin term are included directly in the HF optimization of the radial wave functions. The configuration interaction (CI) basis set included all the configurations of the Layzer complex in addition to the intraconfiguration spin-orbit interaction which introduces mixing between different *LS* states with the same value of *J*. We have used a perturbation approach to determine both the radiative and autoionization rates (A_r and A_a). The energy of the free electron used to calculate the autoionization probabilities depends only on the average energy of the initial and final configurations. The target state is described in a monoconfigurational approach.

A number of theoretical and experimental works have already been achieved on the *K* Auger spectra of neon. Most of the theoretical works have been performed using a single configuration approach either in the Hartree-Fock [30,31] or in the Dirac-Fock formalism [32,33]. Some differences appear between our results and these previous calculations which can be easily explained by the neglect of the correlation effects. We plan to present the complete description of our theoretical results and a systematic comparison with the other theoretical and experimental values in future [34].

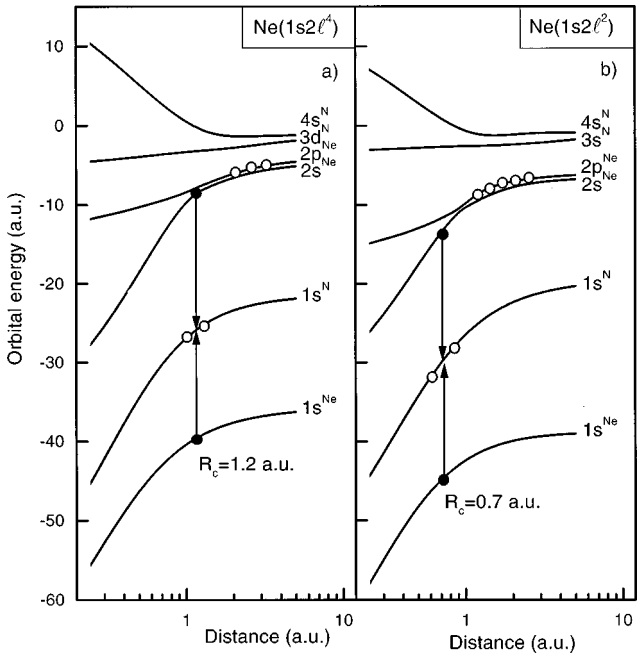

FIG. 6. Molecular-orbital energies for the system $(N+Ne)^{7+}$ evaluated by diagonalization of model matrix elements [27]. Data for (a) three and (b) five spectator electrons. The arrows labeled R_C show the crossings of the corresponding potential curves.

The average Auger yield $\overline{a_K}$ was determined, using a simple arithmetic averaging procedure. The value of about 0.9 was found and assumed to be independent of the collision velocity. Total cross section σ^K for producing a *K* vacancy in the target was then evaluated by dividing σ^a by the quantity $\overline{a_K}$. To explain the role of the spectator electrons during the collision and the dependence of the cross sections on the projectile velocity, calculations were performed within the framework of molecular-orbital (MO) diagrams described in the following section.

IV. MOLECULAR ORBITALS AND POTENTIAL CURVES

The model matrix elements that have been evaluated previously [27] within a screened hydrogenic model (SHM) were used to evaluate the (MO) energies by means of numerical diagonalization. The results for σ orbitals are presented in Fig. 6, which refers to neon with a decreasing number of spectator electrons. At large internuclear distance, the MO energies correlate to the orbital energies of N and Ne. In the entrance channel, the two active electrons occupy the $1s$ and $2l$ ($2s$ in Fig. 6) orbitals of neon. At small internuclear distances, energetic resonance conditions are created for the dielectronic excitation process [Figs. 6(a) and 6(b)]. There, at distance R_C, both active electrons are simultaneously transferred from the target into the $1s$ orbital of nitrogen.

To determine the distance R_C, potential curves were evaluated. These curves are obtained [20] by addition of the MO curves of the associated active electrons. The potential curve of the final configuration $1s^2$ was corrected for orbital relaxation effects, i.e., it was shifted by a constant energy

due to the increase of the binding of the second electron after removal of the first one. It is found that the quantity R_C, which refers also to the curve crossings, is of the order of ~ 1 a.u. At distance R_C, a simultaneous transition of the two active electrons can occur.

For smaller values of n_L ($n_L=0$, 1, and 2), no crossing appears between the entrance channel and the $1s^2$ orbital of nitrogen. Hence, the cross sections cannot be evaluated within the Landau-Zener model [24]. More accurate orbital energies are needed to determine the contribution of the lowest values of n_L.

V. CROSS SECTION CALCULATIONS AND DISCUSSION

The Landau-Zener model [24] was applied at curve crossings R_C for the cross sections σ_{n_L} for producing a K vacancy, after the removal of n_L spectator electrons ($n_L \geqslant 3$) from the target. At a curve crossing with radius R_C the transition probability between initial state (i) and final state (f) is given by [17]

$$p_{if}(b) \approx N_f \frac{2\pi |V_{if}|^2}{v_R(b)\Delta F(R_C)}. \tag{1}$$

In this expression, N_f is the number of final states, b is the impact parameter, v_R is the radial velocity, and $\Delta F(R_C)$ is a measure for the relative inclination of the potential curves at crossing R_C. The dielectronic matrix element $V_{if}(R_C)$ describes the interaction at the curve crossing. It is pointed out that expression (1) is an accurate approximation to the Landau-Zener formula [24] for small perturbations $2\pi |V_{if}|^2 \ll v_R \Delta F(R_C)$.

The quantity V_{if} is defined as $V_{if}=\langle \varphi(1s'2l')|1/|\mathbf{r}_1-\mathbf{r}_2||\varphi(1s^2)\rangle$, where $\varphi(1s'2l')$ and $\varphi(1s^2)$ describe the two active electrons located at the target and the projectile, respectively. According to previous evaluations [2,17], a reasonable value of 0.05 a.u. was retained for V_{if} in our calculations. This value is consistent with evaluations of V_{if} using hydrogenic wave functions for both initial state $1s2l$ and final state $1s^2$ from neon and nitrogen, respectively [35]. The number of final states N_f may be large for open shells produced by removal of outer-shell electrons during the collision. For example, values as high as 30 were suggested in the analysis of the $2pnl'$ configurations populated during the collision $O^{6+}+He$ [17]. Hence, a reasonable value of 10 was taken for N_f.

For finite internuclear distances, the total transfer probability is obtained as

$$P_{n_L}(b)=2p_{if}(b)[1-p_{if}(b)]. \tag{2}$$

Finally the cross section σ_{n_L}, for a fixed value of n_L, is

$$\sigma_{n_L}=c_{n_L}\int_0^{R_c} 2\pi b P_{n_L}(b)\,db. \tag{3}$$

The quantity c_{n_L} is the probability for producing the number n_L of the spectator electrons. To evaluate c_{n_L}, the statistical method described in Ref. [27] was used. In the statistical treatment, multiple vacancy is governed by a binomial distribution. The probability c_{n_L} is expressed using binomial coefficients and depends on the single-particle probability p_L for the removal of L-shell electrons. As mentioned in Sec. III, the mean number $\overline{n_L}$ is ~ 3.5. Hence, $p_L=\overline{n_L}/7$ is nearly equal to 0.5. This result is consistent with the picture that, during the formation of the quasi-molecule, the L-shell electrons are located on both centers. After the collision, the electrons are shared between the two centers with equal probability ($p_L \approx 0.5$).

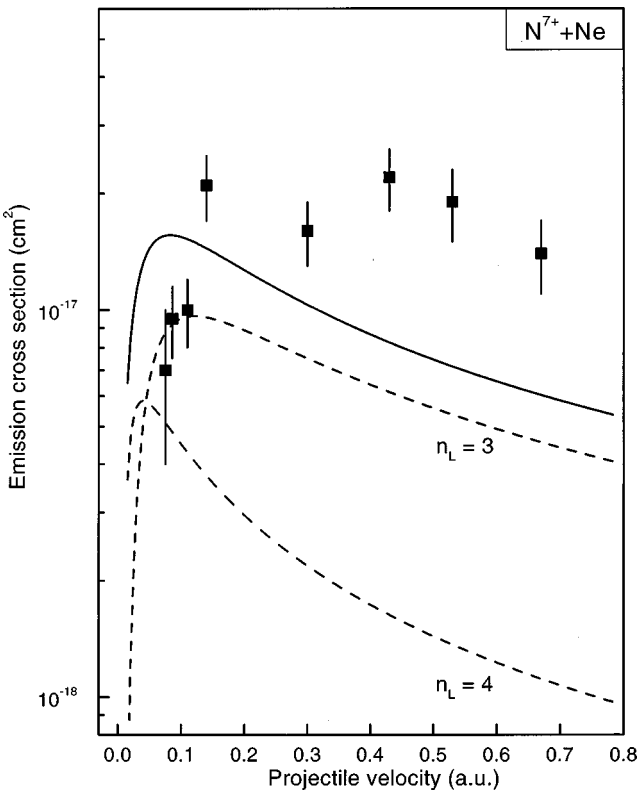

FIG. 7. Experimental cross sections (squares) associated with the production of a neon K vacancy. Dashed lines and full line represent the different contributions σ_{n_L} ($n_L=3$ and 4) and their sum, respectively, obtained from model calculations described in Sec. IV.

In Fig. 7 the results for the largest cross sections σ_{n_L} ($n_L=3$ and 4) are shown as a function of the projectile velocity. The dominance of $n_L=3$ and 4 is consistent with the finding that the mean number $\overline{n_L}$ of spectator electrons is about 3.5 (see Sec. III). At the highest velocities investigated here, the major cross section σ_{n_L} is found to originate from $n_L=3$ (Fig. 7). The mean number $\overline{n_L}$ can be calculated as $\overline{n_L}=\Sigma(n_L\sigma_{n_L})/\Sigma\sigma_{n_L}$. A value of about 3 is found for $\overline{n_L}$ at projectile velocities larger than 0.5 a.u. Hence, the experimental results obtained for $\overline{n_L}$ at these velocities (Table I) are well reproduced by the present calculations. In addition, the relative contribution of $\sigma_{n_L=4}$ compared to that of $\sigma_{n_L=3}$ is found to increase significantly with decreasing projectile velocity (Fig. 7). This result agrees well with the experimental finding that $\overline{n_L}$ increases so as to reach a value of about 4 at velocities lower than 0.1 a.u. (Table I).

Also, in Fig. 7, the full calculation ($\sigma=\Sigma\sigma_{n_L}$) is compared with the experimental cross sections for producing a neon K-shell vacancy. We note a reasonable agreement between the calculation and the experimental results, since the

differences between calculation and experiment do not exceed a factor of ~2. The calculated as well as the experimental cross sections are found to remain relatively large [$\sim(1-2)\times10^{-17}\,\mathrm{cm}^2$] when the projectile velocity decreases from 0.7 a.u. down to 0.1 a.u. (Fig. 7). As qualitatively suggested by the present calculations, the experimental data show that the cross sections are likely to become smaller only at velocities lower than 0.1 a.u. Hence, the present data clearly show that dielectronic excitation is an efficient process for producing *K*-shell vacancies at impact velocities as low as a few tenths of an atomic unit. Further experimental effort is needed to investigate the importance of dielectronic excitation at velocities lower than one-tenth of an atomic unit.

VI. CONCLUSION

In this work *K*-shell vacancy production due to dielectronic excitation is studied experimentally and theoretically. The present study is performed for collisions between bare N^{7+} ions and Ne atoms. Projectile velocities ranging from ~0.1 to 0.7 a.u. are investigated. The method of Auger-electron spectroscopy was used to measure cross sections for producing a *K*-shell vacancy in the multielectron target of Ne. At the low impact velocities investigated here, the cross sections are shown to be of the order of $10^{-17}\,\mathrm{cm}^2$. Since single excitation or ionization plays a negligible role at velocities as low as a few tenths of an a.u., dielectronic excitation governed by the electron-electron interaction is shown to be the unique mechanism that is responsible for the production of *K*-shell vacancies in the present collisions. The remarkable feature is that the process of dielectronic excitation is sufficient enough to give rise to relatively large cross sections for producing *K*-shell vacancies in very slow ion-atom collisions.

The mechanisms for the creation of a *K* vacancy in the target are discussed under the perspective of dynamic electron correlation effects. The discussion is based on molecular-orbital diagrams. From these diagrams, it is seen that the transfer of spectator electrons creates resonance conditions for the transfer of two active electrons via dielectronic excitation. It is found that dielectronic excitation is particularly favored when ~3 target electrons are transferred into an excited state of the projectile.

Using the Landau-Zener model [24] for a number of spectator electrons larger than 2, a relatively large cross section is found for *K*-vacancy production. For smaller values of n_L, the Landau-Zener model cannot be applied. However, calculated total cross sections are in reasonably good agreement with experiment. Observed deviations for total cross section are mostly due to collisional parameters introduced in the model calculation. Improved theoretical work is thus needed to characterize the dielectronic process. In particular, it would be of great interest to distinguish the role of the $2s$- and $2p$-target electrons.

ACKNOWLEDGMENTS

We are much indebted to the staffs of the ECR sources in Berlin and Caen for their assistance. This work was supported by the European Collaboration Research Programs PROCOPE under Contract No. 98089 and TOURNESOL No. 96028. One of us (J.-Y.C.) acknowledges the support of the Alexander von Humboldt Foundation, Germany.

[1] A. Bordenave-Montesquieu, P. Benoît-Cattin, A. Gleizes, S. Dousson, and D. Hitz, J. Phys. B **18**, L195 (1985).
[2] N. Stolterfoht, C. C. Havener, R. A. Phaneuf, J. K. Swenson, S. M. Shafroth, and F. W. Meyer, Phys. Rev. Lett. **57**, 74 (1986).
[3] D. Vernhet, A. Chetioui, J. P. Rozet, C. Stephan, K. Wohrer, A. Touati, M. F. Politis, P. Bouisset, D. Hitz, and S. Dousson, J. Phys. B **22**, 1603 (1989).
[4] C. Harel, H. Jouin, and B. Pons, J. Phys. B **24**, L425 (1991).
[5] Z. Chen, R. Shingal, and C. D. Lin, J. Phys. B **24**, 4215 (1991).
[6] F. Frémont, K. Sommer, D. Lecler, S. Hicham, P. Boduch, X. Husson, and N. Stolterfoht, Phys. Rev. A **46**, 222 (1992).
[7] A. Niehaus, J. Phys. B **19**, 1925 (1986).
[8] M. Boudjema, M. Cornille, J. Dubau, P. Moretto-Capelle, A. Bordenave-Montesquieu, P. Benoît-Cattin, and A. Gleizes, J. Phys. B **24**, 1713 (1991).
[9] H. W. van der Hart, N. Vaeck, and J. E. Hansen, J. Phys. B **27**, 3489 (1994).
[10] H. Bachau, P. Roncin, and C. Harel, J. Phys. B **25**, L109 (1992).
[11] J. P. Desclaux, Nucl. Instrum. Methods Phys. Res. B **98**, 18 (1995).
[12] N. Stolterfoht, C. C. Havener, R. A. Phaneuf, J. K. Swenson, S. M. Shafroth, and F. W. Meyer, Nucl. Instrum. Methods Phys. Res. B **27**, 584 (1987).
[13] H. Winter, M. Mack, R. Hoekstra, A. Niehaus, and F. J. De Heer, Phys. Rev. Lett. **58**, 957 (1987).
[14] N. Stolterfoht, Phys. Scr. **T51**, 39 (1994).
[15] A. Bordenave-Montesquieu, P. Moretto-Capelle, A. Gonzalez, M. Benhenni, H. Bachau, and I. Sánchez, J. Phys. B **27**, 4243 (1994).
[16] F. Frémont, H. Merabet, J.-Y. Chesnel, X. Husson, A. Lepoutre, D. Lecler, G. Rieger, and N. Stolterfoht, Phys. Rev. A **50**, 3117 (1994).
[17] N. Stolterfoht, Phys. Scr. **46**, 22 (1993).
[18] V. V. Afrosimov, Yu S. Gordeev, A. N. Zinoviev, D. H. Rasulov, and A. P. Shergin, in *Electronic and Atomic Collisions, Abstracts of Papers of the IXth International Conference on the Physics of Electronic and Atomic Collisions*, edited by J. S. Risley and R. Geballe (University Press, Seattle, 1975), p. 1066.
[19] R. D. Dubois, N. Stoltefoht, and D. Schneider, in *Inner Shell and X-Ray Physics of Atom and Solids*, edited by D. J. Fabian, H. Kleinpoppen, and L. M. Watson (Plenum, New York, 1981), p. 63.
[20] N. Stolterfoht, Phys. Rev. A **47**, R763 (1993).
[21] F. Frémont, C. Bedouet, J.-Y. Chesnel, H. Merabet, X. Husson, M. Grether, A. Spieler, and N. Stolterfoht, Phys. Rev. A **54**, R4609 (1996).
[22] J.-Y. Chesnel, H. Merabet, X. Husson, F. Frémont, D. Lecler, H. Jouin, C. Harel, and N. Stolterfoht, Phys. Rev. A **53**, 2337 (1996).

[23] J.-Y. Chesnel, B. Sulik, H. Merabet, C. Bedouet, F. Frémont, X. Husson, M. Grether, A. Spieler, and N. Stolterfoht, Phys. Rev. A **57**, 3546 (1998).
[24] C. D. Landau, J. Phys. (Moscow) **2**, 46 (1932); C. Zener, Proc. R. Soc. London, Ser. A **137**, 696 (1932).
[25] M. O. Krause, J. Phys. Chem. Ref. Data **8**, 307 (1979).
[26] N. Stolterfoht, Z. Phys. **248**, 81 (1971); **248**, 92 (1971).
[27] N. Stolterfoht, Phys. Rep. **146**, 315 (1987).
[28] The Auger emission cross section associated with dielectronic excitation at a projectile energy of 35 keV is about 2.1 $\times 10^{-17}\,\mathrm{cm}^2$ (the value of $3\times 10^{-18}\,\mathrm{cm}^2$ reported in our paper [21] was underestimated by a factor of 7).
[29] R. D. Cowan, *The Theory of Atomic Structure and Spectra* (University of California Press, Berkeley, 1981).
[30] D. L. Matthews, B. M. Johnson, and C. F. Moore, At. Data Nucl. Data Tables **15**, 41 (1975).
[31] C. P. Bhalla, Phys. Rev. A **12**, 122 (1975).
[32] R. J. Maurer and R. L. Watson, At. Data Nucl. Data Tables **34**, 185 (1986).
[33] M. H. Chen and B. Craseman, At. Data Nucl. Data Tables **38**, 381 (1988).
[34] N. Zitane and N. Vaeck (unpublished).
[35] J.-Y. Chesnel, Ph.D. thesis, Université de Caen, 1996 (unpublished).